Peer-Reviewed Technical Communication

Sizing Drop Weights for Deep Diving Submersibles Taking Into Account Nonuniform Seawater Density Profiles

Blair Thornton

***Abstract*—This technical communication describes a method to size the drop weights used by submersibles for diving and surfacing taking into account varying seawater density profiles. The method allows consistent diving and surfacing performance to be achieved for differently sized submersible and target dive depths. The conditions that need to be met for safe operation of a submersible are described in this paper. The equations needed to appropriately ballast a platform and size its diving and surfacing drop weights are derived, highlighting some inherent limitations of using a two drop weight method for certain types of mission. The performance of the proposed approach is demonstrated through numerical simulations for different sized submersibles and target depths. The results show the effects of using different design parameters to illustrate some useful patterns and trends that can assist submersible developers and operators predict the effects of environmental and design uncertainties on important operational parameters such as the time taken for diving and surfacing.**

***Index Terms*—Marine vehicles, underwater technology, unmanned autonomous vehicles.**

NOMENCLATURE

A	Projected surface area of a submerged body in the horizontal plane, m^2.
g	Acceleration due to gravity, m/s^2.
C_D	Drag coefficient.
M	Total mass of the submerged body, kg.
M_A	Added mass of the submerged body, kg.
T	Time taken for diving and surfacing, s.
V	Volume of fluid displaced by the submerged body, m^3.
W	Total weight of the submerged body in air, N.
W_{sub}	Weight of the submerged body in air with no drop weights, N.
W'_d	Weight of the submerged body in surface water with both drop weights, N.
W'_o	Weight of the submerged body in water with its surfacing drop weight, N.
W'_s	Weight of the submerged body in surface water with no drop weights, N.
z	Depth, m.
z_{target}	Target depth, m.
$\dot{z}$	Vertical velocity, m/s.
$\dot{z}_{\mathrm{max}}$	Maximum vertical velocity, m/s.
$\dot{z}_{\mathrm{min}}$	Minimum vertical velocity, m/s.
$\ddot{z}$	Vertical acceleration, m/s^2.
β	Aspect ratio of a prolate ellipsoid.
δ	Desired minimum buoyancy in surface water with no drop weights, N.
η	Buoyancy design safety factor.
ρ	Seawater density, kg/m^3.
ρ_b	Seawater density at deepest point in observation, kg/m^3.
$\rho_{\bar{b}}$	Seawater density at desired or average observation depth, kg/m^3.
ρ_s	Seawater density at surface, kg/m^3.
ω_d	Weight of the dive drop weight in seawater, N.
ω_s	Weight of the surface drop weight in seawater, N.

Manuscript received April 1, 2018; revised December 6, 2018 and January 29, 2019; accepted February 1, 2019. This work was supported by EPSRC under Grant EP/S001182/1.

Associate Editor: N. Cruz.

The author is with the Maritime Robotics Laboratory, Southampton Marine and Maritime Institute, Faculty of Engineering and Physical Science, University of Southampton, Southampton SO16 7QF, U.K., and also with the Institute of Industrial Science, The University of Tokyo, Tokyo 155-8503, Japan (e-mail: B.Thornton@soton.ac.uk).

Digital Object Identifier 10.1109/JOE.2019.2898070

I. INTRODUCTION

THIS technical communication outlines a simple method to ballast submersibles and appropriately size the drop weights they use for diving and surfacing taking into consideration varying seawater density profiles. The objective is to provide a practical guide to de-risk the operation of deep-diving untethered submersibles, such as autonomous underwater vehicles (AUVs), that use a two drop weight method for diving and surfacing. This report is not intended to be a review of diving, surfacing, and ballast control methods, but instead prioritizes simplicity and ease of implementation over rigorous modeling and accurate simulation. The method described uses only straightforward equations with input parameters that are easily attained. Simulations are performed to identify the effects of sizing decisions on operationally relevant parameters for different sized submersibles. The trends identified can assist submersible developers and operators gauge the impact of submersible ballasting and drop weight sizing decisions on operational safety under expected levels of environment and design uncertainty.

A key component to achieve safe and energetically efficient operation of submersibles in deep-diving applications is the effective control of buoyancy over a large range of depths. A submersible's buoyancy depends on the density of fluid it displaces and so any change in seawater density has a direct impact on its operation. In extreme cases, such as at the bottom of the Mariana trench, the density of seawater can be as high as 1080 kg/m^3, approximately 6% higher than at the surface, with density increasing as a function of depth by approximately 0.5% per kilometre and also changing with salinity and temperature [1], [2]. The greatest variability in seawater temperature and salinity is seen in the upper part of the water column at depths of $<$1000 m, where the consistency between these parameters at different locations and times increases for larger depths. While a detailed description of the global variability of seawater density is beyond the scope of this paper, the main trends are as follows:

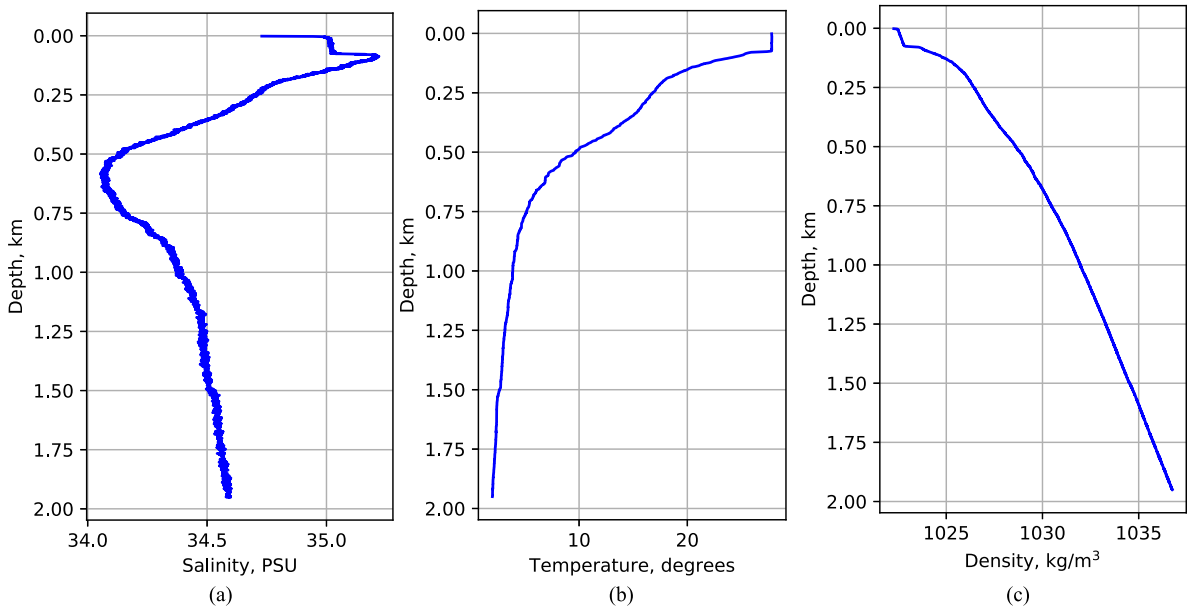

Fig. 1. Example vertical profiles of seawater temperature, calculated salinity, and seawater density in the Northwest Pacific (22°43.7'N 153°16.4'E). The data was collected during the YK17-23C expedition on board the RV Yokosuka using an XCTD-4 expendable conductivity temperature depth profiler (The Tsurumi-Seiki Co., Ltd.). (a) Salinity profile. (b) Temperature profile. (c) Density profile.

- colder water is more dense than warmer water;
- saltier water is more dense than fresher water; and
- higher pressure causes density to increase.

Fig. 1 shows the depth profiles of these seawater parameters measured down to a depth of 2 km in the Northwest Pacific (22°43.7'N 153°16.4'E) in October 2017, where seawater density has been calculated using the UNESCO TEOS10 thermodynamic equation of seawater [3]. Failure to account for changes in seawater density can result in the following:

- a submersible being unable to dive to its target depth;
- increased power consumption and degradation in the quality of data obtained due to inappropriate ballasting during observation; and
- loss of the submersible due to it becoming trapped midwater column unable to surface.

The objective of this paper is to outline a simple method that can account for varying density profiles and demonstrate how these can be used to determine suitable ballast conditions and appropriately size drop weights for reliable deep-diving submersible operations.

The effects of nonuniform vertical seawater density profiles on the operation and safety of submersibles should be considered during their design. Methods to compensate for buoyancy effects include the use of isopycnal hulls [4], passive oil and gas based compensators [5], and active buoyancy control systems [6]. The use of emergency drop weights is a common safety feature on AUVs and gliders [7]. These are released in the event of an emergency, typically by activating a burn wire, cutting power to an electromagnet or corrosion of a galvanic element, to allow a submersible to float to the surface. The purpose of these is to minimize the consequence of low probability but foreseeable abnormalities such as a breached housing, loss of floatation material, a collapsed buoyancy lung, or the submersible becoming trapped on a foreign object. Sizing of these systems is not easily formalized since the requirements vary significantly for different submersible designs and application scenarios. However, there are many examples of buoyancy control being used as part of standard operational workflows. Buoyancy engines are the control device of choice for gliders and floats as they

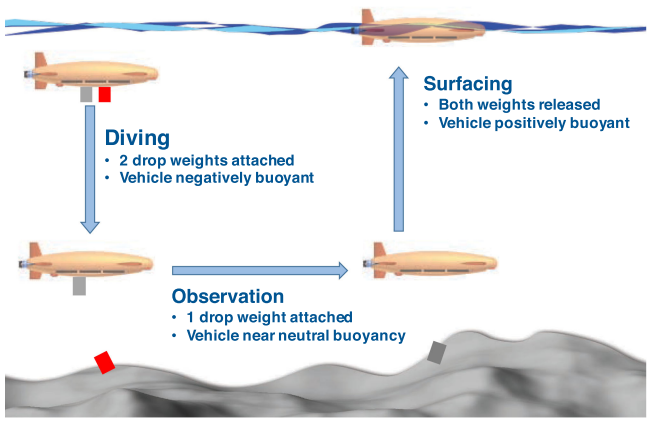

Fig. 2. Schematic representation of diving and surfacing using the two drop weight method.

allow the platforms to perform the repeat vertical profiles required to collect data from the water column. Buoyancy engines typically displace seawater with a low-density oil to adjust their buoyancy, where the resulting buoyancy can be fine-tuned for different seawater densities by varying the displaced volume [7]. Unlike gliders and floats, the submersibles used in seafloor mapping applications typically maintain a constant depth or altitude during observation and their missions often consist of a single dive cycle. For single dive cycle applications reaching depths greater than several hundreds of meters, the two drop weight method, illustrated in Fig. 2, is an effective way to minimize energy consumption and improve the safety of submersible operation. Two electromagnetically retained weights, called the diving and surfacing weights, are mounted on an appropriately ballasted submersible prior to its deployment. This makes the submersible negatively buoyant at the start of its mission so that it can dive without the need to use its actuators. Once the submersible approaches its target observation depth, it releases the diving drop weight. If the drop weight is correctly

TABLE I
EXAMPLES OF FIELD OPERATIONAL AUVS USING THE TWO DROP WEIGHT METHOD

AUV	Type	Mass, kg	Depth rating, m	Source
Tuna-Sand	Hover	278	1,500	[10, 14]
Tuna-Sand 2	Hover	380	2,000	[11]
Hobalin	Hover	270	2,000	[12]
AE2000a	Flight	300	2,000	[13, 14]
AE2000f	Flight	370*	2,000	[13, 14]
BOSS-A	Hover	580	3,000	[15]
Otohime	Hover	842	3,000	[16]
GPAUV	Flight	620	2,000	[17]
SBPAUV	Flight	780	2,000	[17]
ISiMI6000	Flight	809	6,000	[18]
r2D4	Flight	1,800*	4,000	[19]

*Indicates changes resulting from modifications made since the most recent literature.

sized, this allows the submersible to achieve near neutral buoyancy during observation. This is important to prevent unnecessary use of energy overcoming a buoyancy offset and can also have an impact on the quality of certain types of survey data such as low altitude seafloor visual imaging where heavy use of vertical actuators can agitate sediments and degrade image quality [8], [9]. The surfacing drop weight is released at the end of the observation phase of the mission and the submersible surfaces passively under its own buoyancy. The method reduces the amount of energy spent during diving and surfacing and is inherently robust to failure as a loss of power will result in any retained weights being released, allowing the submersible to return to the surface.

The best choice of technology for buoyancy control is application specific. Beyond their inherent fail-safe nature, the major advantage of the two drop weight method compared to buoyancy engines is the large space saving that can be achieved for an equivalent change in net buoyancy by using dense ballast materials like steel and lead with densities of 7800 and 11 340 kg/m^3, respectively. The method can also be easily integrated into existing systems and is typically used by submersibles that dive to depths of 1000 m or more, where self-propelled diving, maintaining of target depth and surfacing can have a major impact on the energy budget. The main limitations of the method are that neutral buoyancy cannot be maintained over a large range of observational depths during a single deployment (e.g., surveys of the slope of a seamount) and it does not allow for multiple descent and ascent cycles. As such, the method is used mainly by deep-diving submersibles used for seafloor mapping. Table I gives some examples of field operational AUVs that use this method together with their mass and depth rating. These range from the relatively compact 2000 m rated Tuna-Sand and Ae2000 series AUVs with masses of 240 to 380 kg, to the medium-sized 6000 m rated ISiMI6000 with a mass of 809 kg and the larger 4000 m rated r2D4 at approximately 1.8 tonnes [10]–[19]. However, despite there being many platforms using the two drop weight method there are no published guidelines for sizing them. Larger drop weights allow for faster diving and surfacing, increasing the proportion of time that can be spent making observations and reducing the risk of a platform being unable to float back to the surface at the end of its mission. However, larger drop weights also require additional floatation to maintain neutral buoyancy during observation and increase the power used by a submersible to retain them. It is therefore important to develop a theoretical basis to dimension the drop weights appropriately and achieve a desired performance tradeoff.

II. METHOD AND ASSUMPTIONS

A competent buoyancy control system used by a submersible for seafloor mapping applications must satisfy the following three functional requirements:

a) be able to return to the surface after its missions and remain afloat with sufficient buoyancy to avoid antenna washover and facilitate recovery;
b) be close to neutral buoyancy at its target observation depth; and
c) be able to dive to its target depth.

The method described in this paper satisfies these requirements taking as input:

- the displacement of the submersible; and
- the seawater density profile;

and an appropriate safety factor, η, which needs to be defined. It is reasonable to assume that for any field operational AUV, the submersible's displacement is known. Seawater density profiles can be determined from standard measurements such as conductivity-temperature and depth (CTD) profiles, and expendable CTD (XCTD) or expendable bathythermograph casts [20], [21]. The following assumptions are made to minimise the number of inputs required by the method:

- contraction and expansion of the submersible's volume is negligible; and
- the volume of the drop weights is small relative to that of the submersible.

These are reasonable as the materials used for pressure vessels (aluminium, titanium vessels, glass domes, ceramics) and floatation (syntactic foam, glass spheres, ceramics) are rigid for most submersibles, where the buoyancy effects of expansion and contraction due to changes in temperature ($<25 \times 10^{-6}$ K^{-1} for the above mentioned materials) and pressure (where housings are generally designed to operate within 0.2% offset yield) are more than an order of magnitude smaller than the changes in seawater density seen during deep-diving operations at sea [22], [23]. Other factors that can influence buoyancy, such as absorption of seawater by floatation foams, are not considered as they occur gradually over time scales larger than a single dive cycle for routine submersible operations [24]. The method considers the weight of the drop weights in seawater to be constant with depth. This is to minimize the number of input terms required by the method as accounting for this effect would require additional information about the drop weights used to be characterised (i.e., their volume or density). While including these effects is not onerous, for drop weights made out of high density materials such as steel or lead, i.e., density $>$ 7800 kg/m^3 comprising just a few percent of the submersible's mass, the relative contribution of the drop weight's varying buoyancy due to changes in seawater density would be in the order of $<1\%$ of the corresponding total buoyancy change of the submersible, and so can reasonably be considered negligible.

The design safety factor, η, is a positive constant defined as the ratio of the desired net buoyancy of the submersible at the surface, δ, and the trimmed weight of the submersible in air without any drop weights

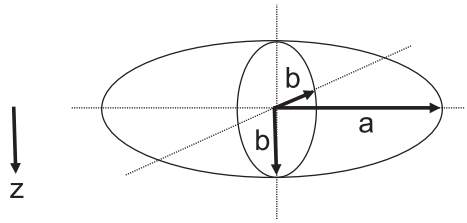

Fig. 3. Prolate ellipsoid used to model the submersible.

attached, W_{sub}, where

$$\eta = \frac{\delta}{W_{\mathrm{sub}}}. \tag{1}$$

Functional requirement a) can be met by satisfying the condition

$$W_s' \leq -\delta. \tag{2}$$

W_s' is the net weight of the submersible in surface seawater once it has released both drop weights and resurfaced, as illustrated by "surfacing" in Fig. 2. The equation can be expanded as follows:

$$W_{\mathrm{sub}} - \rho_s \cdot g \cdot V \leq -\eta \cdot W_{\mathrm{sub}} \tag{3}$$

where the second term is the buoyancy of the submerged body, which displaces a volume V of seawater, where ρ_s is the density of seawater at the surface, and g is the acceleration due to gravity. Typically, it is desirable to have a net buoyancy of between 1% to 5% of the submersible's weight to ensure that the submersible breaks the surface and floats the antennae needed for localization and communication. This corresponds to having an η value between 0.01 and 0.05, where a larger value increases the net buoyancy at the surface. A value of $\eta = 0$ results in the submersible being neutrally buoyant at the surface, which is undesirable as the submersible would not break the surface, making it hard to spot and its antennae for localization and communication would remain immersed and so be ineffective. A small η value would also result in a long period taken to reach the surface, which is undesirable from an operational perspective. Furthermore, any loss of buoyancy (e.g., fracture or chipping of buoyancy material) or increase in weight (e.g., sediments becoming trapped in fairing material or a small leak of a housing) during the mission would result in the submersible becoming unable to return to the surface. Since both ρ_s and V are known, the appropriate weight in air to ballast the submersible to achieve a desired value of η can be determined as follows:

$$W_{\mathrm{sub}} \leq \frac{\rho_s \cdot g}{1+\eta} \cdot V \tag{4}$$

While this yields an inequality, if an appropriate value of η is selected W_{sub}, i.e., the submersible weight without any drop weights, can be trimmed accordingly to achieve the minimum weight in air that satisfies (4).

Functional requirement b) can be met by satisfying the condition

$$W_o' = 0. \tag{5}$$

During observation the submersible retains only its surfacing ballast having released its dive ballast at the end of the preceding diving phase, as illustrated by "observation" in Fig. 2. Equation (5) can be expanded as follows:

$$W_{\mathrm{sub}} + \omega_s - \rho_{\bar{b}} \cdot g \cdot V = 0 \tag{6}$$

where ω_s is the weight of the surfacing drop weight in seawater. The third term represents the buoyancy of the submersible, where the displaced seawater has density $\rho_{\bar{b}}$ at the desired observational depth. In situations where the depth of observations varies, such as for surveys on the slopes of seamounts [9], the average value of seawater density at the observational depth should be used in (6). Since W_{sub} can be determined from (4), (6) can be rearranged to determine the appropriate weight in seawater for the surfacing drop weight as follows:

$$\omega_s = \rho_{\bar{b}} \cdot g \cdot V - W_{\mathrm{sub}}. \tag{7}$$

Functional requirement c) can be met by satisfying the condition

$$W_d' \geq \delta. \tag{8}$$

W_d' is the net weight of the submersible in surface seawater when it has both drop weights attached, as illustrated by "diving" in Fig. 2. This can be expanded as follows:

$$W_{\mathrm{sub}} + \omega_d + \omega_s - \rho_b \cdot g \cdot V \geq \eta \cdot W_{\mathrm{sub}} \tag{9}$$

where ω_d is the weight of the dive drop weight in seawater. Since seawater density increases with depth, it is important to ensure that the submersible is still capable of diving when its buoyancy is at its maximum, i.e., at the greatest depth of operation where the density of seawater is ρ_b. For near constant observational depths $\rho_b = \rho_{\bar{b}}$, whereas for observations at varying depths, $\rho_b > \rho_{\bar{b}}$. This equation can be rearranged to determine the size of the diving drop weight in seawater as follows:

$$\omega_d \geq (\eta - 1)\, W_{\mathrm{sub}} + \rho_b \cdot g \cdot V - \omega_s \tag{10}$$

where substituting in (7) yields

$$\omega_d \geq \eta \cdot W_{\mathrm{sub}} + (\rho_b - \rho_{\bar{b}}) \cdot g \cdot V. \tag{11}$$

For constant depth observations, where $\rho_b = \rho_{\bar{b}}$, this further simplifies to the following form:

$$\omega_d \geq \eta \cdot W_{\mathrm{sub}}. \tag{12}$$

A submersible can be appropriately ballasted and its drop weights sized by solving (4), (7), and (11) [or (12) for near constant depth observations], where choosing the minimum values of W_{sub} and ω_d, which satisfy (4) and (11) [or (12)], ensures that both the diving and surfacing rates are similar. The rate itself and robustness to uncertainty in the submersible's volume V, and change of seawater density is determined by the choice of η.

TABLE II
SIMULATION PARAMETERS

Simulated conditions	Submersible V, m^3	η	Target depth, km
Discrete V and η continuous depth (see Fig. 5-6)	0.3, 0.8, 1.8	(0), 0.01, 0.02, 0.03, 0.04, 0.05	0 to 11 (continuous)
Discrete V, η and depth (see Fig. 7-8)	0.3	0.01, 0.02, 0.03, 0.04, 0.05	1, 6
Continuous V, discrete η and depth (see Fig. 9, 11)	0.1 to 2.0 (continuous)	0.01, 0.02, 0.03, 0.04, 0.05	1, 3, 6, 11
Continuous V, discrete η and depth (see Fig.10)	0.1 to 2.0 (continuous)	0.01, 0.02, 0.03, 0.04, 0.05	1, 6

III. SIMULATION

The diving and surfacing performance of submersibles using the two drop weight method sized as described in Section II is simulated

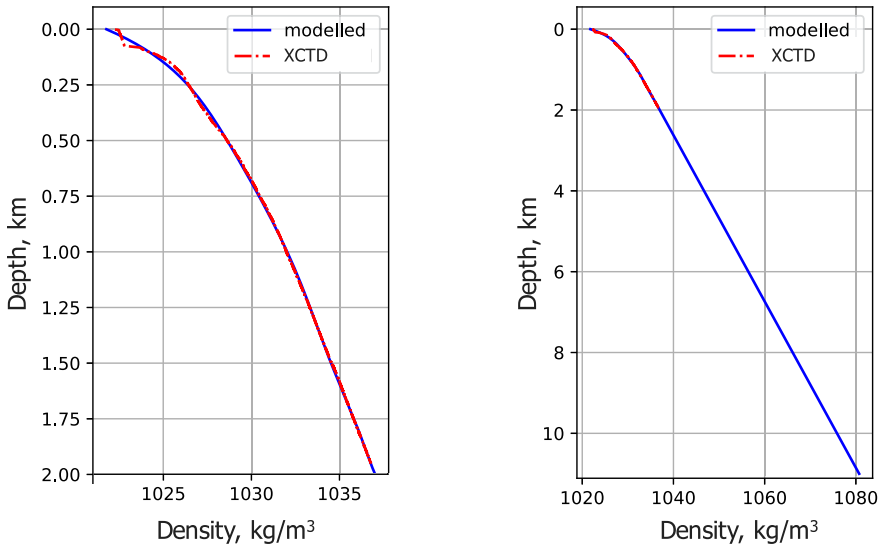

Fig. 4. Seawater density profile (red) determined from *in situ* measurements, as described in Fig. 1, and that modeled (blue) and extrapolated to full ocean depth. (a) Overlapping region of the model. (b) Full model down to 12 km.

TABLE III
RATIO OF WEIGHT OF SUBMERSIBLE (IN AIR) TO SUBMERSIBLE VOLUME, WHERE THE MINIMUM SIZE OF THE DIVING DROP WEIGHT (IN SEAWATER) ω_d IS GIVEN BY ηW_{sub} IN (12)

η	0	0.01	0.02	0.03	0.04	0.05
$(W_{\mathrm{sub}}/V)/g$	1.022	1.012	1.002	0.992	0.982	0.973

The ratio W_{sub}/V has been divided by acceleration due to gravity to give the value in terms of equivalent specific gravity.

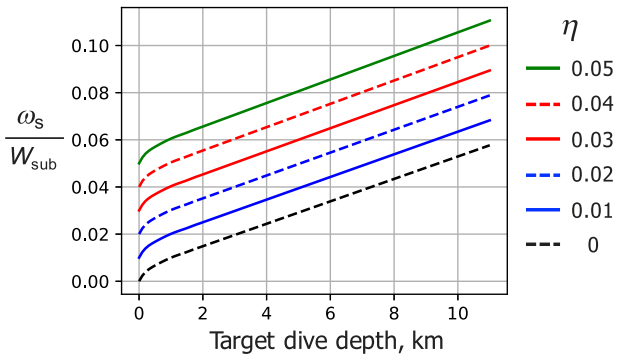

Fig. 5. Size of surfacing drop weights in seawater nondimensionalized by submersible weight in air as a function of target dive depth for various values of η.

for a range of vehicle sizes and target depths. In the simulations, the diving drop weight is released when the submersible reaches its target observation depth, and it is assumed that the target observation depth is constant within each simulated run. The simulations consider submersibles between 0.1 and 2 m^3, i.e., approximately 100 to 2000 kg, as this range covers a large proportion of ocean going AUVs that use the two drop weight method (see Table I). Performance curves are generated for submersible volumes of 0.3, 0.8, and 1.8 m^3, representing small, medium, and large submersibles that use the two drop weight methods respectively. These illustrate the change in diving and surfacing times over a depth range of 0 and 11 km for values of η varied between 0 (theoretical minimum but in practical terms unsafe) and 0.05. The change in diving and surfacing rates and the net buoyancy during vertical transits are also computed for different observational depths for a 0.3 m^3 submersible. This size of submersibles is chosen as small submersibles are more sensitive to the choice of η in terms of the diving and surfacing velocities. The relative buoyancy and the relative change in velocities during diving and surfacing, however, do not change for different sized submersibles as long as their form factor and the values of η chosen remain the same. Table II summarises the simulation parameters used in this paper.

The simulation takes as input the vertical seawater density profile, the volume of the submersible and the choice of η value. The submersible is modeled as a prolate ellipsoid with an aspect ratio a/b or β, of 5, as shown in Fig. 3. The drag coefficient of the submersible in the vertical direction is computed using strip theory, where the contribution of thin strips that make up the submersible are integrated [25]. The Reynolds number remains $<5 \times 10^5$ for all simulated conditions, indicating that a constant C_D approximation can be used, where the drag coefficient of each thin section is modeled as a two-dimensional circular cross section with $C_D = 1.17$. Integrating over the length of the submersible yields a normalised vertical C_D of 1.00, acting on the projected surface area of the body in the horizontal plane, A, which lies normal to the vertical direction of motion. The assumption is made that the submersible dives and surfaces normal to its major axis and passively under its own weight and buoyancy as described by the following dynamic equation:

$$(M + M_A) \cdot \ddot{z} + \frac{1}{2} \cdot C_D \cdot \rho(z) \cdot A \cdot \dot{z} \cdot |\dot{z}| = \sum W - \rho(z) \cdot g \cdot V. \tag{13}$$

This has been modified from [26] to account for the increase in seawater density with depth. M and M_A are the total mass and added mass of the submerged body. The term ΣW is the total weight of the submersible in each drop weight configuration, i.e., $W_{\mathrm{sub}} + \omega_d + \omega_s$ during diving, $W_{\mathrm{sub}} + \omega_d$ during observation, and W_{sub} during surfacing as illustrated in Fig. 2. The following additional assumptions are made in the simulation:

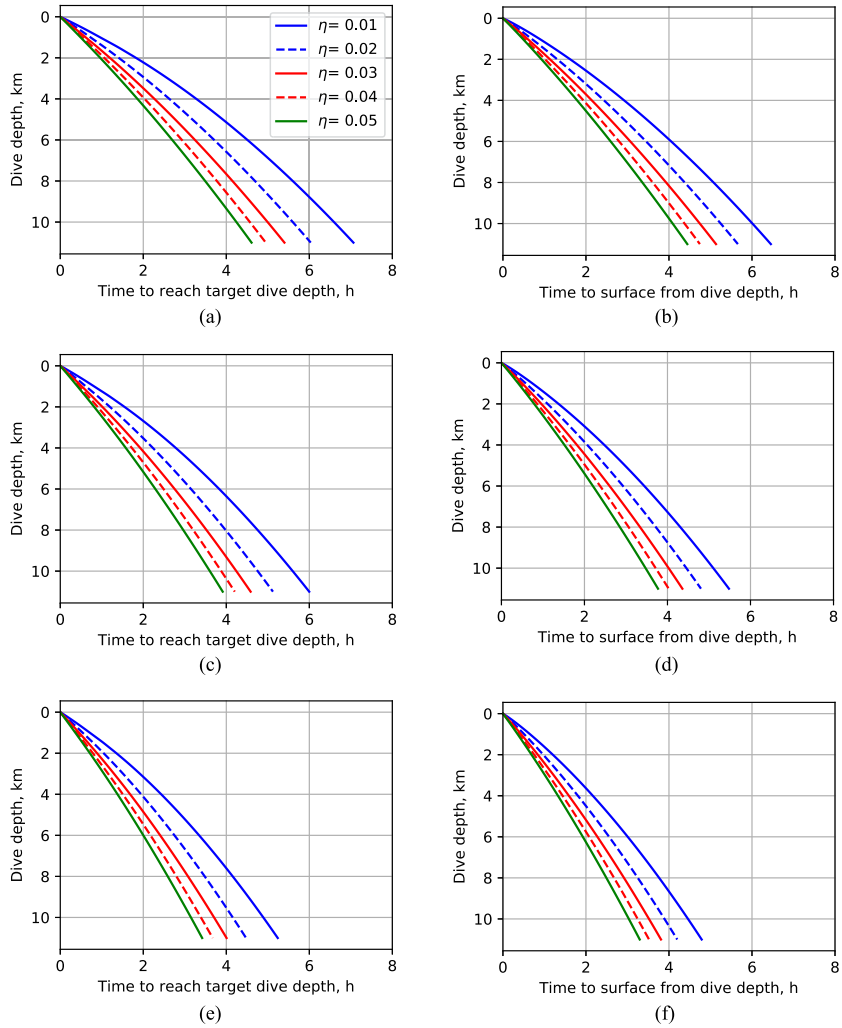

Fig. 6. Diving and surfacing times as a function of target dive depths for submersibles with a displacement of (a) and (b) 0.3 m^3. (c) and (d) 0.8 m^3. (d) and (e) 1.8 m^3.

- the vertical component of current is negligible; and
- the contribution of transient effects on the dynamics is negligible.

These are reasonable since the vertical components of ocean currents are known to be in the order of 10^{-6} m/s in the water column [27], which is five orders of magnitude lower than the diving and surfacing rates considered relevant in this paper. Furthermore, the changes in the hydrostatic forces that decelerate or accelerate the submersible's motion in the vertical direction only change gradually as it dives or surfaces over large distances. The seawater density profile is modeled by fitting the data shown in Fig. 1, where the initial 1.5 km is modeled using a 6th order polynomial and beyond 2 km, the density is linearly extrapolated down to full ocean depth. In the transition region between 1.5 and 2 km, a weighted average is used to achieve a smooth transition between the two models. The modeled seawater density profile is shown in Fig. 4.

For drop weights designed as outlined in this paper using the minimum values required to satisfy (4), (7), and (12), respectively, the maximum and minimum vertical velocities can be derived from (13), where the maximum velocity during diving occurs at the surface and can be determined as follows:

$$\dot{z}_{d_{\max}} = \left[\frac{2\cdot g}{C_D\cdot A}\cdot\left(\frac{\eta}{1+\eta}+\frac{\rho_b}{\rho_s}-1\right)\right]^{\frac{1}{2}} V^{\frac{1}{2}} \tag{14}$$

where the minimum vertical velocity during diving occurs at the deepest target dive depth, which can be calculated as:

$$\dot{z}_{d_{\min}} = \left[\frac{2\cdot g}{C_D\cdot A}\cdot\left(\frac{\eta}{1+\eta}\cdot\frac{\rho_s}{\rho_b}\right)\right]^{\frac{1}{2}} V^{\frac{1}{2}}. \tag{15}$$

Similarly the maximum velocity during surfacing occurs at the target depth, immediately after releasing the surfacing ballast and can be determined as follows:

$$\dot{z}_{s_{\max}} = -\left[\frac{2\cdot g}{C_D\cdot A}\cdot\left(1-\frac{\rho_s}{\rho_b\,(1+\eta)}\right)\right]^{\frac{1}{2}} V^{\frac{1}{2}} \tag{16}$$

where the minimum vertical velocity during surfacing occurs at the surface and can be calculated as:

$$\dot{z}_{s_{\min}} = -\left[\frac{2\cdot g}{C_D\cdot A}\cdot\left(1-\frac{1}{1+\eta}\right)\right]^{\frac{1}{2}} V^{\frac{1}{2}}. \tag{17}$$

For a prolate ellipsoid with an arbitrary aspect ratio β = a/b, (14) to (17) can be expressed by the following power law relation with V, where for diving:

$$\dot{z}_{d_{\max}} = \left[\frac{4.028}{C_D^{\frac{1}{2}}\cdot\beta^{\frac{1}{6}}}\cdot\left(\frac{\eta}{1+\eta}+\frac{\rho_b}{\rho_s}-1\right)^{\frac{1}{2}}\right] V^{\frac{1}{6}} \tag{18}$$

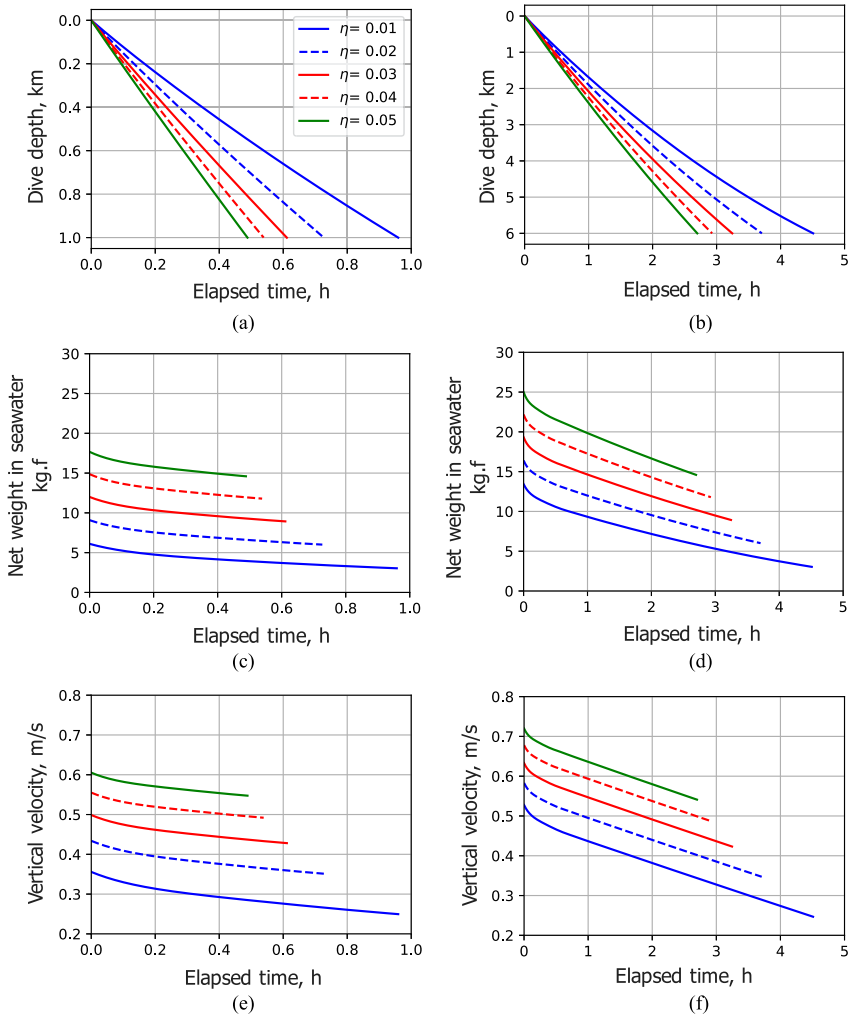

Fig. 7. Plots showing the (a) and (b) dive profiles, (c) and (d) net weight, and (e) and (f) velocity profiles for target depths of 1 and 6 km respectively for a submersible of displacement 0.3 m^3.

and

$$\dot{z}_{d_{\min}} = \left[\frac{4.028}{C_D^{\frac{1}{2}} \cdot \beta^{\frac{1}{6}}} \cdot \left(\frac{\eta}{1+\eta} \cdot \frac{\rho_s}{\rho_b}\right)^{\frac{1}{2}}\right] V^{\frac{1}{6}}. \tag{19}$$

Similarly for surfacing

$$\dot{z}_{s_{\max}} = -\left[\frac{4.028}{C_D^{\frac{1}{2}} \cdot \beta^{\frac{1}{6}}} \cdot \left(1 - \frac{\rho_s}{\rho_b\,(1+\eta)}\right)^{\frac{1}{2}}\right] V^{\frac{1}{6}}, \tag{20}$$

and

$$\dot{z}_{s_{\min}} = -\left[\frac{4.028}{C_D^{\frac{1}{2}} \cdot \beta^{\frac{1}{6}}} \cdot \left(1 - \frac{1}{1+\eta}\right)^{\frac{1}{2}}\right] V^{\frac{1}{6}}. \tag{21}$$

Equations (18) to (21) can be used to verify that there are sufficient margins for safe operation allowing for any uncertainty in the input parameters (i.e., V and ρ) for any target depth of observation.

IV. Results

Table III gives the ratios of W_{sub}/V that satisfy (4) for discrete values of η, where the minimum size of the diving drop weight to satisfy (12) has been used in each case. These values remain constant with the target dive depth and are constant for different values of V. Fig. 5 shows the nondimensionalized size of surfacing drop weights calculated using (7), which varies as a function of the target dive depth.

Fig. 6(a) to (f) shows the respective times taken to dive and surface for different target depths and values of η, where $\eta = 0$ has been omitted since in any practical scenario, any level of uncertainty would massively impact the results. Each plot shows the depth of the submersible together with the corresponding net buoyancy and velocities for different sized submersibles and η values. W_{sub}, ω_d, and ω_s have been sized to satisfy (4), (7), and (12) for each set of conditions with minimal redundancy. The trend observed is that for a given target depth and value of η, the diving and surfacing times are faster for large submersibles than for smaller ones, where the relative difference is bigger for small values of η. This is because volume, and so buoyancy, is a third-order function of their dimensions, whereas their drag is a second-order function, resulting in larger buoyancy or weight to drag ratios for large submersibles and so faster diving and surfacing rates.

Figs. 7 and 8 show the respective diving and surfacing profiles of a 0.3 m^3 submersible for target depths of 1 and 6 km. Figs. 7, 8(a), and (b) show the descent and ascent profiles with (c) and (d) showing the net weights in seawater, and (e) and (f) showing the vertical velocities. Larger values of η lead to larger net weights and so faster diving and surfacing. Figs. 7 and 8(c) to (f) show that the net weight changes due to the increased buoyancy of the submersible as seawater

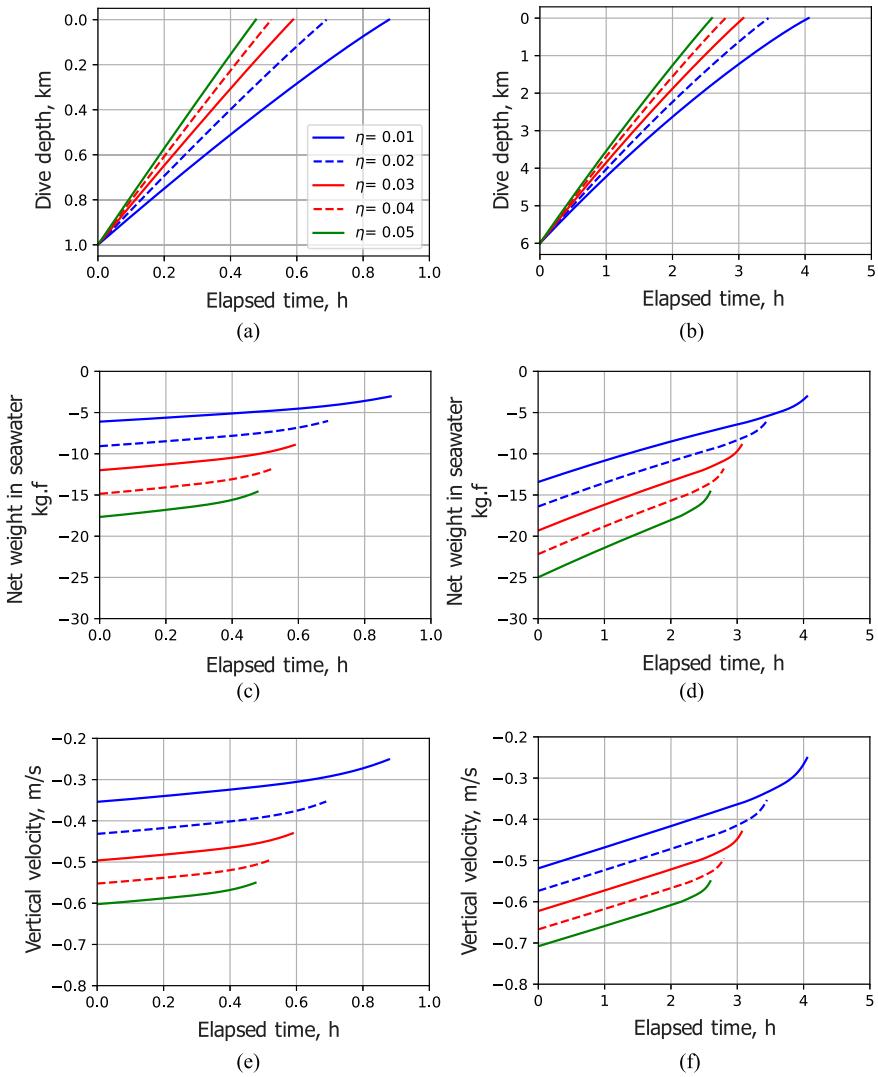

Fig. 8. Plots showing the (a) and (b) surfacing profiles, (c) and (d) net weight, and (e) and (f) velocity profiles for target depth of 1 and 6 km respectively for a submersible with a displacement of 0.3 m^3.

density increases with depth. The change in buoyancy drives a change in vertical velocity with some contribution from the change in drag due to the varying seawater density. As would be expected from the seawater density profile in Fig. 4, the relative change in net weight and vertical velocity are more pronounced for the deeper condition due to the larger seawater density range. During the descent, diving becomes more difficult as the submersible depth increases due to an increased buoyancy as the displaced seawater becomes more dense. Conversely, during the submersible's ascent, its buoyancy decreases as it approaches the surface and the displaced seawater becomes less dense.

Fig. 9 shows that the relative change in net weight and diving and surfacing rates is independent of submersible volume and can be determined from the target dive depths and the value of η. The curves show that in all cases, there is diminishing return in terms of limiting net weight and vertical velocity change for increased values of η. For small η values, the relative change over the range of depths the submersibles pass through approaches 100%, at which point the submersible would be unable to reach its target depth when diving, or unable to reach the surface for recovery. The diving and surfacing performance for small values of η is also significantly more sensitive to any uncertainty in the input parameters, i.e., submersible volume and seawater density.

From Figs. 9 and 10, it can be seen that the maximum and minimum vertical velocities are almost equal in magnitude, with opposite signs for diving and surfacing respectively. While the relative change in net weight and vertical velocity are independent of the size of the submersible, Fig. 10 shows that the absolute vertical velocities change with submersible size and target dive depths of 1 and 6 km respectively. The maximum vertical velocity, which can be obtained from (17) and (19), occurs near the surface during diving, as seen in Fig. 10(a) and (c), and at the deepest point of the dive during surfacing, as seen in Fig. 10(b) and (d). For any given displaced volume, larger η values result in an increase in the maximum and minimum vertical velocity for both diving and surfacing. Similarly, for any given η value, an increase in the displaced volume results in an increase in the maximum and minimum vertical velocity for both diving and surfacing.

While the velocity profiles and so the time taken for diving and surfacing, T_d and T_s, depend on the density profile of the seawater (see Figs. 7 and 8), the diving and surfacing times can be roughly estimated

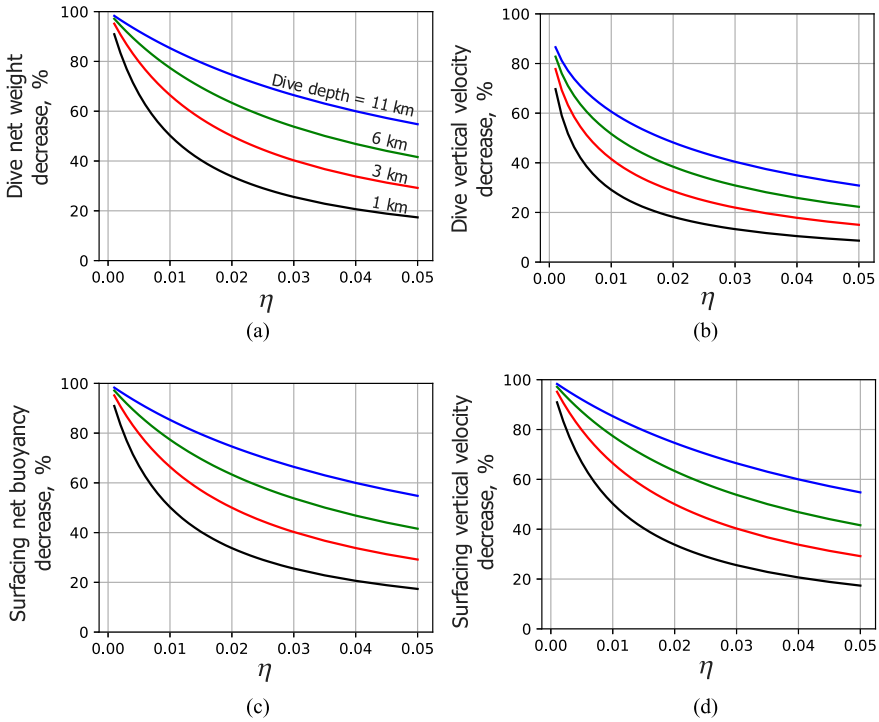

Fig. 9. Relative change in (a) net weight and (b) vertical velocity when the submersible reaches its target depth, and the relative change in (c) buoyancy and (d) vertical velocity when surfacing when the submersible reaches the surface.

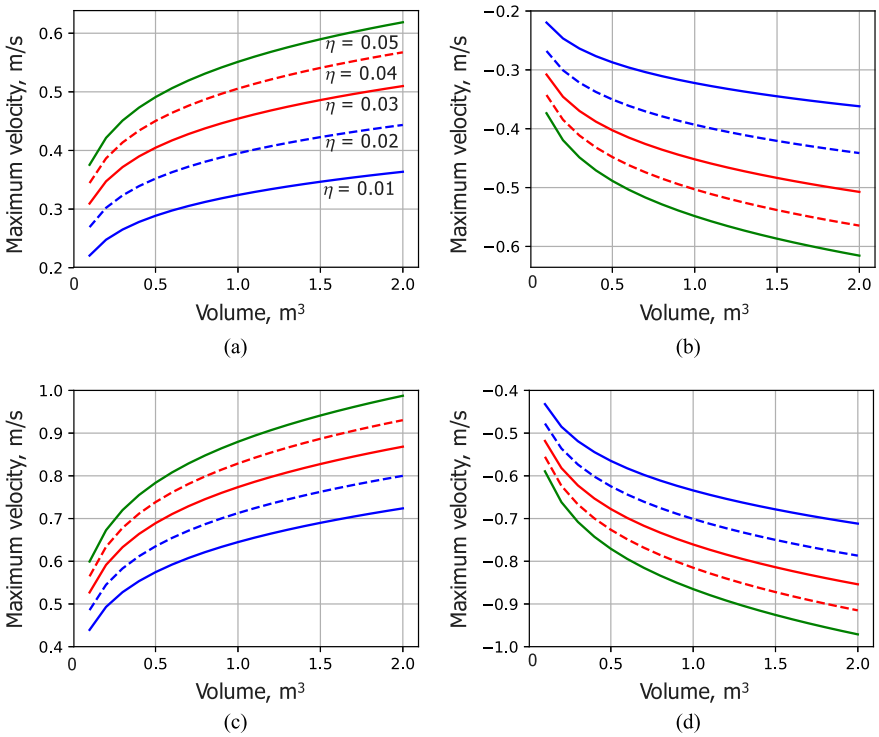

Fig. 10. Plots of (a) and (c) diving and (b) and (d) surfacing maximum velocities for a target depth of 1 and 6 km respectively, as a function submersible displacement for different values of η.

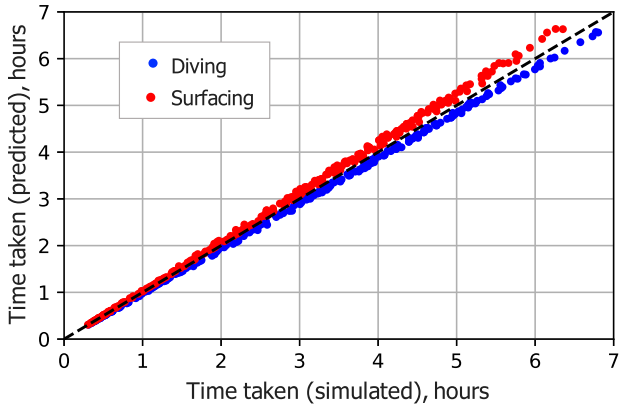

Fig. 11. Correlation between time taken to dive and surface simulated using (13) and that predicted by the simplified relationship in (22) for 300 randomly assigned combinations of η, V, and target depths within the ranges given in Table II for β values between 2 and 10.

from the following relationships:

$$T_d = \frac{z_{\text{target}}}{0.5\left(\dot{z}_{d_{\max}} + \dot{z}_{d_{\min}}\right)} \qquad T_s = \frac{z_{\text{target}}}{0.5\left(\dot{z}_{s_{\max}} + \dot{z}_{s_{\min}}\right)} \quad (22)$$

where the maximum and minimum velocities determined using (18) to (21) should be used to determine the time taken for diving and surfacing respectively. Fig. 11 compares the output of (22) for 300 randomly assigned combinations of η, V, and target depths within the ranges given in Table II for β values between 2 and 10 with the corresponding output of simulations that solve the dynamic model given in (13). The result shows that while (22) tends to under predict the dive time and overpredict the surfacing time, it remains within a 5% of the simulated output, with the advantage that it can be directly computed given the desired η value and seawater densities at the surface and target depth for an arbitrary size submersible, without the need for numerical simulation.

V. Conclusion

This paper has outlined a simple method that can be used to appropriately ballast a submersible and size drop weights for the two drop weight method for diving and surfacing. The method requires the volumetric displacement of the submersible to be known alongside the vertical seawater density profile and target dive depth, where all of these parameters can be determined with relative ease. The results show that larger values of η result in smaller relative changes in the buoyancy and vertical velocity during diving and surfacing in realistic environments that have depth varying seawater density profiles. While larger values of η are favourable, the diminishing return in terms of the robustness of passive diving and surfacing for very large values of η should be considered when determining an appropriate value of η. The excess in buoyancy required for high η values is expensive, especially for deep diving submersibles, due to the high cost of sufficiently pressure rated buoyancy material. Furthermore, heavy drop weights can lead to an increased power consumption as they are typically held using electromagnets. The simulations show that small submersibles require larger η values to achieve the same diving and surfacing times as submersibles that are similarly shaped but larger in size. The relative change in diving and surfacing rates and net weight/buoyancy due to changes in seawater density, however, is independent of the submersible's size. The simulations illustrate the relative gains in the potential time spent making observations through faster diving and surfacing that is offered by having larger η values, and a simple method to approximate the times required for diving and surfacing is described. The simulated results and equations derived in this paper can help submersible developers and operators gauge the impact of sizing design decisions and any uncertainty in the input parameters on diving and surfacing performance when using the two drop weight method. Ultimately, the choice of η depends on the uncertainty that exists in parameters such as the volumetric displacement of the submersible, its ballasting and the seawater density profiles, which must be balanced against the risks an operator is willing to take during the operation of a submersible and the value they assign to rapid diving and surfacing.

Acknowledgment

The author would like to thank Dr. T Ura of the Kyushu Institute of Technology, Japan, and Dr. G. Weymouth and A. Bodenmann of the University of Southampton, UK, for their careful consideration and valuable advice during the preparation this paper.

References

[1] S. C. Riser *et al.*, "Fifteen years of ocean observations with the global Argo array," *Nature Clim. Change*, vol. 6, pp. 145–153, 2016, doi: 10.1038/nclimate2872.

[2] C. Wang, S. Dong, and E. Munoz, "Seawater density variations in the North Atlantic and the Atlantic meridional overturning circulation," *Clim. Dyn.*, vol. 34, pp. 953–968, 2010, doi: 10.1007/s00382-009-0560-5.

[3] IOC, SCOR, and IAPSO, "The international thermodynamic equation of seawater–2010: Calculation and use of thermodynamic properties," Manual and Guides 56, Intergovernmental Oceanographic Commission, UNESCO, Paris, France, 2010. [Online]. Available: http://www.TEOS-10.org

[4] C. C. Eriksen *et al.*, "Seaglider: A long-range autonomous underwater vehicle for oceanographic research," *IEEE J. Ocean. Eng.*, vol. 26, no. 4, pp. 424–436, Oct. 2001. doi: 10.1109/48.972073

[5] M. E. Furlong, D. Paxton, P. Stevenson, M. Pebody, S. D. McPhail, and J. Perrett, "Autosub long range: A long range deep diving AUV for ocean monitoring," in *Proc. IEEE/OES Auton. Underwater Veh.*, 2012, pp. 1–7, doi: 10.1109/AUV.2012.6380737

[6] S. A. Woods, R. J. Bauer, and M. L. Seto, "Automated ballast tank control system for autonomous underwater vehicles," *IEEE J. Ocean. Eng.*, vol. 37, no. 4, pp. 727–739, Oct. 2012, doi: 10.1109/JOE.2012.2205313

[7] J. Hunt, "Global inventory of AUV and glider technology available for routine marine surveying," in *Proc. Southampton UK NERC Mar. Renewable Energy Knowl. Exchange*, 2013, p. 153, doi: 10.25607/OBP-25

[8] M. Johnson-Roberson, O. Pizarro, S. B. Williams, and I. Mahon, "Generation and visualization of large-scale three-dimensional reconstructions from underwater robotic surveys," *J. Field Robot.*, vol. 27, pp. 21–51, 2010, doi: 10.1002/rob.20324

[9] A. Bodenmann, B. Thornton, and T. Ura, "Generation of high-resolution three-dimensional reconstructions of the seafloor in color using a single camera and structured light," *J. Field Robot.*, vol. 34, pp. 833–851, 2017, doi: 10.1002/rob.21682

[10] T. Nakatani *et al.*, "AUV "TUNA-SAND" and its Exploration of hydrothermal vents at Kagoshima Bay," in *Proc. Oceans MTS/IEEE Kobe Techno-Ocean*, 2008, pp. 1–5, doi: 10.1109/OCEANSKOBE.2008.4531099

[11] Y. Nishida *et al.*, "Development of an autonomous underwater vehicle with human-aware robot navigation," in *Proc. Oceans MTS/IEEE Monterey*, 2016, pp. 1–4. doi: 10.1109/OCEANS.2016.7761471

[12] A. Okamoto *et al.*, Development of Hovering-type AUV "HOBALIN" for exploring seafloor hydrothermal deposits," in *Proc. Oceans MTS/IEEE Monterey*, 2016, pp. 1–4. doi: 10.1109/OCEANS.2016.7761452

[13] K. Asakawa, J. Kojima, Y. Kato, S. Matsumoto, and N. Kato, "Autonomous underwater vehicle aqua explorer 2 for inspection of underwater cables," in *Proc. IEEE Int. Underwater Technol. Symp.*, 2000, pp. 242–247, doi: 10.1109/UT.2000.852551

[14] T. Ura, R/V Kaiyo Cruise Report KY12-13, JAMSTEC Document Catalogue, Jpn. Agency Mar. Earth Sci. Technol., Yokosuka, Japan, Tech. Rep. KY12-13. 2012. [Online]. Available: http://www.godac.jamstec.go.jp/catalog/data/doc_catalog/media/KY12-13_all.pdf

[15] Y. Nishida *et al.*, "Development of an autonomous underwater vehicle for survey of Cobalt-rich manganese crust," in *Proc. Oceans MTS/IEEE*, Washington, DC, USA, 2015, pp. 1–5, doi: 10.23919/OCEANS.2015.7404606

[16] T. Nakatani *et al.*, "Working-AUV "Otohime" and its sea trials at Sagami Bay," in *Proc. IEEE Int. Underwater Technol. Symp.*, 2013, pp. 1–5. doi: 10.1109/UT.2013.6519903

[17] B. Kim, P. Lee, B. Jun, J. Park, and H. Shim, "Design and implementation of control architecture for the ISiMI6000 Autonomous Underwater Vehicle," in *Proc. IEEE/OES Auton. Underwater Veh.*, 2012, pp. 1–5, doi: 10.1109/AUV.2012.6380727

[18] K. Sawada *et al.*, "Development and sea trial of the compact cruising type AUV system," in *Proc. IEEE Underwater Technol.*, 2017, pp. 1–5, doi: 10.1109/UT.2017.7890311

[19] T. Ura *et al.*, "Dives of AUV "r2D4" to Rift Valley of central Indian mid-ocean ridge system," in *Proc. IEEE Oceans*, Aberdeen, U.K., pp. 1–6, doi: 10.1109/OCEANSE.2007.4302392

[20] W. C. Thacker and O. E. Esenkov, "Assimilating XBT data into HYCOM," *J. Atmos. Ocean. Technol.*, vol. 19, pp. 709–724, 2001, doi: 10.1175/1520-0426(2002)019<0709:AXDIH>2.0.CO;2

[21] B. Biescas, B. R. Ruddick, M. R. Nedimovic, V. Sallare's, G. Bornstein, and J. F. Mojica, "Recovery of temperature, salinity, and potential density from ocean reflectivity," *J. Geophys. Res. Oceans*, vol. 119, pp. 3171–3184, 2014, doi:10.1002/2013JC009662

[22] J. Lachambrea, E. Mairea, J. Adriena, and D. Choqueuse, "In situ observation of syntactic foams under hydrostatic pressure using X-ray tomography," *Acta Materialia*, vol. 61, pp. 4035–4043, 2013, doi: 10.1016/j.actamat.2013.03.017

[23] J. R. Calvert and R. A. Farrar, *An Engineering Data Book*. New York, NY, USA: Red Globe Press, 1998, pp. 112.

[24] X. Lefebvre, V. Sauvant-Moynot, D. Choqueuse, and P. Chauchot, "Durability of syntactic foams for deep offshore insulation: Modelling of water uptake under representative ageing conditions in order to predict the evolution of buoyancy and thermal conductivity," *Oil Gas Sci. Technol.—Rev. IFP*, vol. 64, pp. 165–178, 2009, doi: 10.2516/ogst/2008053

[25] J. N. Newman, *Marine Hydrodynamics*. Cambridge, MA, USA: MIT Press, 1977, p. 418.

[26] T. Fossen, *Guidance Control of Ocean Vehicles*. Hoboken, NJ, USA: Wiley, 1994, p. 496.

[27] X. Liang, M. Spall, and C. Wunsch, "Global ocean vertical velocity from a dynamically consistent ocean state estimate," *J. Geophys. Res. Oceans*, vol. 122, pp. 8208–8224, 2017, doi: 10.1002/2017JC012985

Blair Thornton received the B.Eng. degree in naval architecture and the Ph.D. degree in underwater robotics from the University of Southampton, Southampton, U.K., in 2002 and 2006, respectively.

During his Ph.D., he spent two years with the Underwater Robotics & Application Laboratory, Institute of Industrial Science, University of Tokyo, where he continued his research, rejoining the University of Southampton in 2016. During this time, he has participated in more than 50 ocean research expeditions (28 of which as a Principal Investigator) and has spent more than 380 days at sea. He is currently an Associate Professor with the University of Southampton and with an adjunct position with the University of Tokyo, Tokyo, Japan. He is dedicated to fielding systems in real environments and overcoming bottlenecks in the flow of information from data collection through to human insight. His research interests focus on developing scalable methods for visual and *in situ* chemical seafloor observation through improved sensing and autonomy.